

Sustainable Seawater Desalination by Permeate Gap Membrane Distillation Technology

Farzaneh Mahmoudi¹, Mohammad E. Pishbin, Saeed Dehghani¹, Abhijit Date¹,
Aliakbar Akbarzadeh¹

¹Energy CARE Group, School of Aerospace, Manufacturing and Mechanical Engineering, RMIT
University, Melbourne (Australia)

Abstract

Membrane distillation (MD) as a thermally driven process with moderate operating temperatures is a known effective technology for salt-water desalination. In this research, the permeate gap membrane distillation configuration (PGMD), as a novel sustainable MD design having internal heat recovery characteristics, is introduced, designed and the system performance investigated in terms of permeate water flux rate and specific thermal energy consumption (STEC). The experimental results show that, increasing the feed flow rate from 0.1 to 1.1 L/min for the feed salinity in a range of (0–30) ppt, led to increasing the fresh water flux from 2 to 12 kg/m²h, however STEC of the system also showed an increase and varied in a range of 1000 and 2500 kWh/m³.

Furthermore, a single node theoretical model is developed and the modeling results validated with experimental values. It is concluded, optimization of the MD module performance to improve internal heat recovery and produce higher fresh water rate would be achievable by adjusting the effective membrane surface area and feed flow rate.

Keywords: Sustainable desalination, permeate gap membrane distillation, specific thermal energy consumption, permeate flux rate

1. Introduction

According to the World Water Council, 17% of the world population will be living in short of the fresh water supply by 2020 ([Charcosset, 2009](#)). Therefore, the demand for alternative sustainable water sources including ground water, desalinated water and recycled water increased in recent years and thus, the implementation of desalination plants is growing on a large scale. Fresh water can be derived from sea water by evaporation processes e.g., multi-stage flash (MSF), multi-effect distillation (MED) or by membrane based processes, including reverse osmosis (RO), electro dialysis (ED) and membrane distillation (MD).

Membrane distillation is a separation process which involves phase change (liquid-vapour equilibrium) across a hydrophobic, highly porous membrane. In contrast to most membrane separation processes, which are isothermal and have driving forces as trans membrane hydrostatic pressures, concentrations, electrical or chemical potentials, MD is a non-isothermal process.

The commercially developed RO technology consumes high electrical energy normally ranging from 6 to 12 kWh/m³ that is presently being generated from non-renewable and polluting fossil fuels ([Bai et al.](#)). In contrast, MD is a thermal desalination process using lower top temperature (80 °C or less) with respect to the traditional thermal desalination processes.

However, the MD process is still under study and the lack of experimental data has indicated that there is a need for more comprehensive research in this field. The central issues are the external energy source for MD units, lack of MD membranes and fabrication of modules for each MD configuration. Overall, optimization of MD plants is required in order to reach higher MD performance and to decrease energy consumption ([Meindersma et al., 2006](#)), an appropriate redesign of the MD module is demanded in order to achieve mass transfer improvement and to increase the membrane surface area per module volume. Moreover, the energy source of the MD process is an

important issue for commercialization of this technology as a sustainable process. Membrane distillation associated with renewable energy is considered to be a highly promising process, especially for situations where low-temperature solar, waste or other heat is available. The STEC of MD systems varies based on the module configuration, setup scale and operating condition. A wide dispersion of reported values is observed in literatures for STEC, which ranges from 1 to 9000 kWh/m³ (Khayet, 2013).

Generally direct contact membrane distillation (DCMD) as depicted in Fig. 1-left is the most studied MD configuration (Alkhubiri et al., 2012). In DCMD the membrane is in direct contact with the feed solution on one side and the permeate on the other side with the temperature difference across the two sides of the membrane as the process driving force. A novel introduced configuration of MD, is called PGMD which by creating a third channel for produced fresh water via an impermeable film on the permeate side, the cold fluid in the condenser side separates from the permeate and therefore it could be any other liquid like saline feed water. The permeate is extracted from the highest module position, so that the gap between the membrane and the impermeable film fills with permeate during the operation (Fig. 1- right).

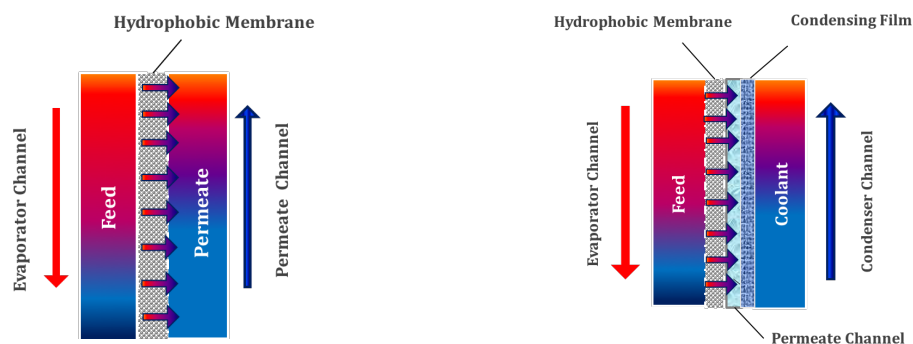


Fig. 1. Left: DCMD configuration; Right: PGMD module arrangement with internal heat recovery

In recent years, some commercial MD modules in different configurations have been developed. (Zaragoza et al., 2014) made a comparison among the most advanced commercial MD prototype technologies with different configurations (air gap, permeate gap and vacuum) and different structures including plate-and-frame and spiral wound. Concerning comparing different MD configuration, Cipollina et al. (Cipollina et al., 2012) also developed a lab scale plate-and-frame membrane distillation module for solar energy seawater desalination and investigated three different channel configurations during this research, including free air gap, permeate-gap and partial vacuum air gap. Winter et al. also developed and optimized MD setup with lowest STEC to reduce the external energy demand of the system, with a 10 m² spiral wound PGMD configuration (Winter et al., 2012).

In this paper, by considering the result of comprehensive literature review regarding recent projects in MD field, an experimental approach by designing and developing a lab scale PGMD system configuration is followed to provide a good estimation of the most important characteristic value of a MD setup, including permeate flux, STEC, GOR and its dependency to the modular design and particularly operating conditions. Furthermore the numerical modeling of the heat and mass transfer phenomena in this configuration is studied and a single node theoretical model is developed using some simplifying assumption and the modeling results validated with comparing to the experimental data

2. Laboratory scale PGMD system experimental rig

A novel optimized experimental approach was based on a lab scale plate-and-frame PGMD module with 0.12 m² effective membrane area. The hydrophobic PTFE membrane, with 0.22 μm nominal pore size and (140 - 200) μm thickness, with an effective surface area (760 * 160) mm², was applied. This plastic PP film had a thermal conductivity similar to that of the PTFE membrane. The permeate channel was separated from the condenser

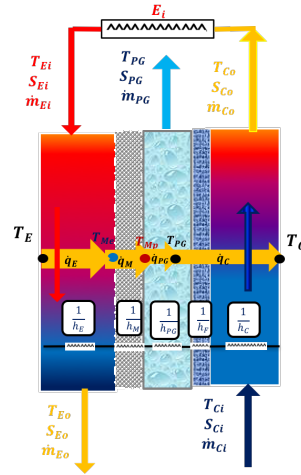


Fig. 3. Single node approach for mathematical modeling of PGMD module

To model the PGMD system, the above assumptions, heat and mass conservation laws in all channels and the five main thermal resistances between evaporator and condenser channels, as shown in Fig. 3 are considered. In addition, by defining the known variables including: T_{Ci} , T_{Ei} , \dot{m}_{Ci} , \dot{m}_{Ei} , S_{Ci} and S_{Ei} which are respectively temperature ($^{\circ}\text{C}$), mass flow rate (kg/s) and salinity (g/kg) at the condenser and evaporator channels inlets, governing equations are developed. It is also required to specify the membrane properties, bulk conditions and module geometry in order to carry out numerical modeling.

The convective heat flux from the evaporator channel to the membrane surface is expressed in Eq. 1:

$$\dot{q}_E = h_E \left(\frac{T_{Ei} + T_{Eo}}{2} - T_{Me} \right) \quad (1)$$

Where, \dot{q}_E is the evaporator channel heat flux (W/m^2), h_E is the heat transfer coefficient at the evaporator channel ($\text{W}/\text{m}^2\text{K}$). T_{Ei} and T_{Eo} are respectively the temperatures at the evaporator channel inlet and outlet and T_{Me} is the temperature at the evaporator side of the membrane surface.

The heat transfer rate from the membrane surface \dot{q}_M arises from the latent heat of the produced vapour flux and the heat transferred by conduction across both the membrane matrix and the gas-filled membrane pores (Khayet, 2011).

Also

$$\dot{q}_M = \frac{K_m}{\delta_m} (T_{Me} - T_{Mp}) + J_p h_{fg} \quad (2)$$

In this equation T_{MP} is the membrane surface temperature at the permeate gap side, h_{fg} is the water vaporization enthalpy (kJ/kg), K_m and δ_m are the membrane thermal conductivity (W/mK) and thickness (m) respectively. J_p ($\text{Kg}/\text{m}^2\text{s}$) (based on Eq. 3) is defined as a function of partial vapour pressure on the two sides of the membrane and of the membrane mass transfer coefficient (C_m).

$$J_p = C_m (P_{v,sw\epsilon} - P_{v,swp}) \quad (3)$$

For the applied membrane samples with specified structure and under the system operating condition, the dominant mass transfer mechanism is defined as a combination of Knudsen and molecular diffusion ($0.01 < Kn < 1$) (Schofield et al., 1987, Alklaibi and Lior, 2006, Alkudhiri et al., 2012, Nakoa et al., 2014). Figures for membrane mass transfer coefficient (C_m) also was in a range of $3 \times 10^{-7} < C_m < 5 \times 10^{-7}$ kg/Pa m²s for (30 - 80) °C temperature range and assuming atmospheric pressure in the membrane pores, which was in close agreement with some reported values (Winter, 2014, Swaminathan et al., 2016, Dow et al., 2016, Kullab, 2011).

Based on the assumptions made, the produced permeate is considered stagnant in the permeate channel, so that the heat transfer from the gap takes place only in the form of conduction calculable by Eq. 5.

$$\dot{q}_{PG} = \frac{1}{\frac{\delta_{PG}}{2K_{PG}}} (T_{Mp} - T_{PG}) \quad (4)$$

In this equation, T_{PG} is the permeate temperature at the permeate gap, K_{PG} (W/mK) and δ_{PG} (m) are the permeate gap thermal conductivity and thickness, respectively.

Moreover, the heat is transferred from the permeate gap to condenser channel by a series combination of thermal resistances including permeate channel and impermeable polymeric film and condenser side thermal resistances. Therefore, the condenser channel heat flux (\dot{q}_C) is defined as below:

$$\dot{q}_C = \frac{1}{\frac{\delta_{PG}}{2K_{PG}} + \frac{\delta_F}{K_F} + \frac{1}{h_C}} (T_{PG} - \frac{T_{Ci} + T_{Co}}{2}) \quad (5)$$

Similarly, in this equation h_C (W/m²K) is the heat transfer coefficients at the impermeable polymeric film and condenser channel, K_F (W/mK) and δ_F (m) are the impermeable polymeric film thermal conductivity and thickness, respectively, T_{Ci} and T_{Co} are the temperatures at the condenser channel inlet and outlet, respectively.

Considering the energy balance correlations for both evaporator and condenser channels and the total membrane surface area (A_m), Eq. 6 and 7 could be assumed respectively for the evaporator channel and condenser channel heat fluxes (\dot{q}_{hot} and \dot{q}_{cold}).

$$\dot{q}_{cold} = \frac{\dot{m}_{Ci} C_{pC} (T_{Co} - T_{Ci})}{A_m} \quad (6)$$

$$\dot{q}_{hot} = \frac{\dot{m}_{Ei} C_{pE} (T_{Eo} - T_{Ei})}{A_m} \quad (7)$$

Given the assumption of a steady state condition, it may be concluded that:

$$\dot{q}_E = \dot{q}_M = \dot{q}_{PG} = \dot{q}_C = \dot{q}_{cold} = \dot{q}_{hot} \quad (8)$$

Solving the 7 main equations (1 to 7) using the Matlab Equation solver, the 7 unknown variables (T_{Me} , T_{MP} , T_{PG} , T_{Co} , T_{Eo} , J_p , \dot{q}), as depicted in the mathematical modelling schematic, may be calculated. Furthermore, to be able describe the performance of a MD system, permeate flux (J_p), STEC and GOR parameters are investigated as the most important characteristic values which are defined as:

The permeate flux J_p could be defined by dividing the permeate output rate \dot{m}_{PG} (kg/s) to the total membrane area (A_m):

$$J_p = \frac{\dot{m}_{PG}}{A_m} \quad (9)$$

The quantity q_{STEC} is the amount of total energy input (E_i) to produce 1 m³ of fresh water ([Sanmartino et al., 2016](#)). In this equation \dot{V}_p is the produced distillate rate (m³/s).

$$q_{STEC} = \frac{E_i}{\dot{V}_p} = \frac{\dot{m}_{Ei} C_p (T_{Ei} - T_{Co})}{\dot{V}_p} \quad (10)$$

The GOR is an indication of how well the total energy input to the system is utilized to produce fresh water:

$$GOR = \frac{\dot{m}_{PG} h_{fg}}{E_i} \quad (11)$$

4. Results and discussion

In this section, the effect of different feed water flow rates and salinities on internal heat recovery through the system, besides the most important characteristic values including permeate flux, STEC, and GOR are presented.

The effect of feed water salinity on internal heat recovery is depicted in Fig. 4-left. As seen in this figure, the amount of internal heat recovery inside the cold flow channel, decreased by increasing the feed flow rate within the system operating condition. Increasing of feed flow rate, lead to the lower feed residence time in the flow channels, so there was less time for heat transfer between hot and cold channels, so the temperature rises in condenser channel was less significant ([Xu et al., 2016](#), [Khayet, 2011](#), [Guillén-Burrieza et al., 2015](#)). In addition, as seen in this figure, by increasing the feed water salinity from fresh water feed (nearly 0% salinity) to seawater salinity (around 30 ppt) and then up to a higher value to 130 ppt, the temperature rise in the condenser channel (internal heat recovery rate) decreased. This pattern could be explained by the negative effect of salinity on permeate flux rate, which leads to a lower amount of released latent heat of condensation at the higher salinity.

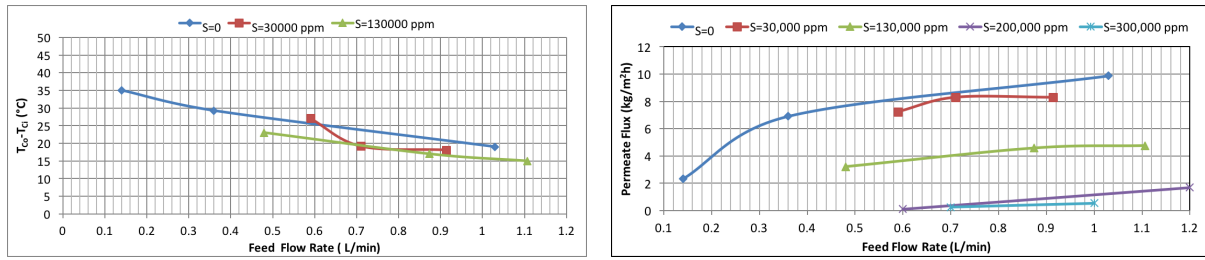


Fig.4. Left: Fresh water temperature rise ($T_{Co}-T_{Ci}$) by internal heat recovery through the membrane, Right; Permeate flux at different feed flow rates and salinities, test condition: $T_{Ci}=15^{\circ}\text{C}$, $T_{Ei}=82^{\circ}\text{C}$

The effect of the feed flow rate on permeate flux is also shown in Fig. 4-right. As it is seen in this graph by increasing the feed flow rate, the permeate flux increases. For fresh water feed (assuming zero percent salinity), increasing feed flow rate from 0.14 to 1.03 L/min, led to approximately 400 per cent increase in the permeate flux. For a feed sample with 130 ppt (nearly four times seawater salinity), doubling the feed flow rate led to a similar upward trend on produced distillate rate. That is the, J_p increases from approximately 3 to 5 $\text{kg}/\text{m}^2\text{h}$ (nearly 70 per cent increase). This effects may be explained by the higher turbulence in the flow channel at the higher feed flow rate, associated with higher value for the Reynolds number, which improved the heat transfer rate in flow channels and reduced the temperature polarization effect on the two sides of the membrane surface. As a result, the temperature difference across the membrane surface increased, leading to higher permeate flux.

Fig. 4-left also presents the effect of salinity on permeate flux, which shows a decrease in permeate water flux for saline water compared to the fresh water feed case. The produced distillate rate decreased significantly for high salt concentration (200-300) ppt, which is near the saturated state of saline feed water. As seen in this graph, for a feed sample with 20 ppt salinity and at nearly 1 L/min flow rate, the distillate flux decreased to less than 2 $\text{kg}/\text{m}^2\text{h}$.

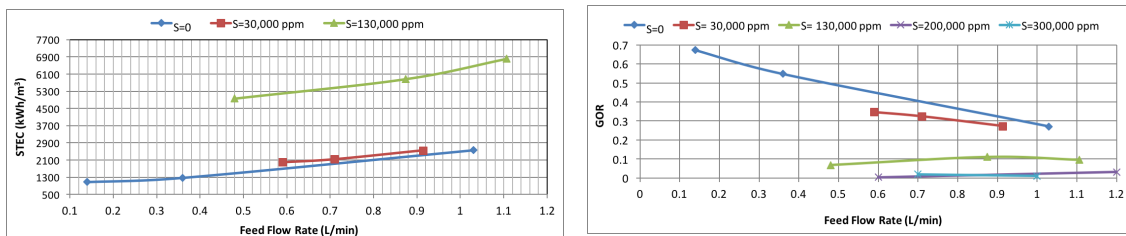


Fig.5. Left: STEC Right; GOR at different feed flow rates and salinities, test condition: $T_{Ci}=15^{\circ}\text{C}$, $T_{Ei}=82^{\circ}\text{C}$

The effect of feed flow rates on STEC of the system is shown in Fig. 5-left. The results show that by increasing the feed flow rate, the required amount of thermal energy will increase. High feed flow rate leads to shorter feed residence time in the flow channel, therefore a less efficient sensible heat recovery in condenser channel is possible. As a result, for a similar operating condition, T_{Co} decreases and the amount of external heat demand (STEC) to reach the designed value for T_{Ei} , increases. On the other hand, as seen in Fig. 4, right by increasing the feed flow rate, the permeate flux rate increases (higher value of \dot{V}_p in Eq. 10). However, the overall the effect of higher energy demand is not completely compensated by higher permeate flux, so the STEC values increase at the higher feed flow rate. As is seen from this figure, at higher feed salinities, the STEC is also increases because of the lower permeate output at higher salinities which is also confirmed by previous studies (Winter et al., 2011, Cipollina et al., 2012).

Gained output ratio is an alternative representation of the STEC and for analyzing the thermal efficiency of the desalination systems may be used to quantify the module’s capability for internal heat recovery. As is explained by Winter et al. (Winter et al., 2012), in MD desalination systems because of heat loss by conduction through the MD module, all the thermal energy input can not be applied to the evaporation process and the GOR must be less than 1. However, in ideal MD systems with optimum internal heat recovery with high surface area for heat transfer

between hot and cold fluids, a higher value of GOR would be possible.

As investigated in this study and illustrated in Fig. 5-right, by increasing feed flow rate and feed water salinity, GOR values show a downward trend. The maximum value achieved for GOR was approximately one, which confirmed the high heat loss rate through the lab scale module and insufficient internal heat recovery by the developed PGMD module with the geometry described. A longer module flow channel with higher membrane surface area will provide more efficient sensible heat recovery leading to a higher GOR value and so develop a more thermally efficient MD system (Winter et al., 2012).

Based on the developed theoretical model described in section 3, the influences of feed flow rate and salinity on two important desalination system characteristic of permeate flux (J_p) and internal heat recovery rate ($T_{Co}-T_{Ci}$) are plotted and the results are compared with the measured values. Figs. 6 shows a good comparison between experimental results and theoretical values for produced fresh water rate and for internal heat parameters. Comparison is made for feed flow rate in the range 0.1 to 1.1 L/min and with three inlet feed salinities of approximately (0, 30 and 130) ppt. As is evident from these graphs, values obtained from numerical modeling using heat and mass balance equations and using the Matlab Equation solver for a single node model, as explained in the mathematical model development section, are in good agreement with experimental measured values. The developed theoretical model could be applied as a reliable tool, to design the geometrical configuration of an optimized PGMD system based on simulation of the system performance.

The theoretical study also provides a basis for developing a more efficient PGMD module by estimating the effect of system parameters including module length, feed flow rate and temperature on the main output parameters including permeate flux rate and STEC .

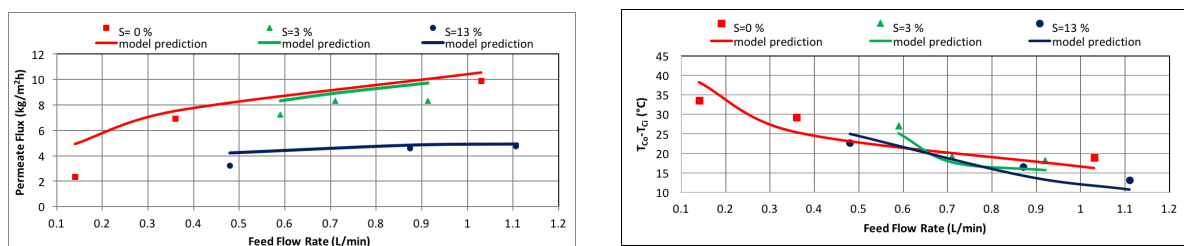


Fig. 6 Theoretical and experimental value comparison for influence of feed flow rate and salinity on: Left: permeate flux; Right: internal heat recovery at condenser channel (Bai et al.)

5. Conclusion

A lab scale plate-and- frame PGMD module with 0.12 m² effective membrane area has been developed and tested. A set of experimental test has been performed to investigate the designed MD module's main characteristics in different operating condition including feed flow rate and salinity. Under the designed system conditions, $T_{Ci}=15$ °C, $T_{Ei}=82$ °C, feed flow rate in range of 0.1 to 1.1 L/min and feed salinity in a range of (0 - 30) ppt the permeate flux varied from (2-12) kg/m²h, specific thermal energy consumption was between 1000 and 2500 kWh/m³ and GOR was below 1.

The experimental results show that lower feed flow rate provides higher residence time and lower STEC (higher GOR). Operation at lower STEC is also achievable by increasing flow channel length and providing more contact time between feed stream and membrane surface leading to higher heat recovery and lower external energy demand of the system. However, working at low feed flow rate and high membrane surface area results in lower permeate flux and higher investment cost respectively. Therefore, to develop a sustainable PGMD configuration design, from the design point of view, the module length and effective membrane surface area need to be optimized in order to improve internal heat recovery rate in the system and so reduce the external energy demand, especially in the situation where the external energy source derives from non-renewable fossil fuels. In conclusion, the research results provides a reliable technical data for a scaled up PGMD module characterization to design a more

efficient and sustainable desalination system via minimizing the thermal energy demand of the system and also producing higher distillate rate.

6. References

- ALKHUDHIRI, A., DARWISH, N. & HILAL, N. 2012. Membrane distillation: A comprehensive review. *Desalination*, 287, 2-18.
- ALKLAIBI, A. & LIOR, N. 2006. Heat and mass transfer resistance analysis of membrane distillation. *Journal of Membrane Science*, 282, 362-369.
- BAI, F., AKBARZADEH, A. & SINGH, R. *A Novel System Of Combined Power Generation And Water Desalination Using Solar Energy*, Solar09, the 47th ANZSES Annual Conference.
- CHARCOSSET, C. 2009. A review of membrane processes and renewable energies for desalination. *Desalination*, 245, 214-231.
- CIPOLLINA, A., DI SPARTI, M. G., TAMBURINI, A. & MICALE, G. 2012. Development of a Membrane Distillation module for solar energy seawater desalination. *Chemical Engineering Research and Design*, 90, 2101-2121.
- DOW, N., GRAY, S., LI, J.-D., ZHANG, J., OSTARCEVIC, E., LIUBINAS, A., ATHERTON, P., ROESZLER, G., GIBBS, A. & DUKE, M. 2016. Pilot trial of membrane distillation driven by low grade waste heat: Membrane fouling and energy assessment. *Desalination*, 391, 30-42.
- GUILLÉN-BURRIEZA, E., ALARCÓN-PADILLA, D.-C., PALENZUELA, P. & ZARAGOZA, G. 2015. Techno-economic assessment of a pilot-scale plant for solar desalination based on existing plate and frame MD technology. *Desalination*, 374, 70-80.
- KHAYET, M. 2011. Membranes and theoretical modeling of membrane distillation: a review. *Adv Colloid Interface Sci*, 164, 56-88.
- KHAYET, M. 2013. Solar desalination by membrane distillation: Dispersion in energy consumption analysis and water production costs (a review). *Desalination*, 308, 89-101.
- KULLAB, A. 2011. Desalination Using Membrane Distillation Experimental and Numerical Study Doctoral Thesis .
- MEINDERSMA, G. W., GUIJT, C. M. & DE HAAN, A. B. 2006. Desalination and water recycling by air gap membrane distillation. *Desalination*, 187, 291-301.
- NAKOA, K., DATE, A. & AKBARZADEH, A. 2014. A research on water desalination using membrane distillation. *Desalination and Water Treatment*, 56, 2618-2630.
- SANMARTINO, J. A., KHAYET, M. & GARCÍA-PAYO, M. C. 2016. Chapter 4 - Desalination by Membrane Distillation A2 - Hankins, Nicholas P. In: SINGH, R. (ed.) *Emerging Membrane Technology for Sustainable Water Treatment*. Boston: Elsevier.
- SCHOFIELD, R. W., FANE, A. G. & FELL, C. J. D. 1987. Heat and mass transfer in membrane distillation. *Journal of Membrane Science*, 33, 299-313.
- SWAMINATHAN, J., CHUNG, H. W., WARSINGER, D. M., ALMARZOOQI, F. A., ARAFAT, H. A. & LIENHARD V, J. H. 2016. Energy efficiency of permeate gap and novel conductive gap membrane distillation. *Journal of Membrane Science*, 502, 171-178.
- WINTER, D. 2014. Membrane Distillation A Thermodynamic, Technological and Economic Analysis.
- WINTER, D., KOSCHIKOWSKI, J. & RIPPERGER, S. 2012. Desalination using membrane distillation: Flux enhancement by feed water deaeration on spiral-wound modules. *Journal of Membrane Science*, 423-424, 215-224.
- WINTER, D., KOSCHIKOWSKI, J. & WIEGHAUS, M. 2011. Desalination using membrane distillation: Experimental studies on full scale spiral wound modules. *Journal of Membrane Science*, 375, 104-112.
- XU, J., SINGH, Y. B., AMY, G. L. & GHAFFOUR, N. 2016. Effect of operating parameters and membrane characteristics on air gap membrane distillation performance for the treatment of highly saline water. *Journal of Membrane Science*, 512, 73-82.

ZARAGOZA, G., RUIZ-AGUIRRE, A. & GUILLÉN-BURRIEZA, E. 2014. Efficiency in the use of solar thermal energy of small membrane desalination systems for decentralized water production. *Applied Energy*, 130, 491-499.

7. Appendix: Nomenclature

Quantity	Symbol	Unit
Membrane surface area	A_m	m^2
Membrane mass transfer coefficient	C_m	
Condenser channel specific heat capacity	C_{pC}	$J\ kg^{-1}\ K^{-1}$
Evaporator channel specific heat capacity	C_{pE}	$J\ kg^{-1}\ K^{-1}$
Hydraulic diameter	D_h	m
Total energy input	E_i	W
Gained output ratio	GOR	
Specific heat of vaporization	h_{fg}	$J\ kg^{-1}$
Heat transfer coefficient at the condenser channel	h_C	$Wm^{-2}\ K^{-1}$
Heat transfer coefficient at the evaporator channel	h_E	$Wm^{-2}\ K^{-1}$
Heat transfer coefficient at the impermeable polymeric film	h_F	$Wm^{-2}\ K^{-1}$
Heat transfer coefficient at the permeate gap	h_{pG}	$Wm^{-2}\ K^{-1}$
Heat transfer coefficient at the membrane	h_M	$Wm^{-2}\ K^{-1}$
Permeate flux	J_p	$Kg\ m^{-2}\ s$
Evaporator channel thermal conductivity	K_E	$W\ m^{-1}\ K^{-1}$
Membrane thermal conductivity	K_m	$W\ m^{-1}\ K^{-1}$
Permeate gap thermal conductivity	K_{pG}	$W\ m^{-1}\ K^{-1}$
Module length	L	m
Feed flow rate	\dot{m}_f	$kg\ s^{-1}$
Inlet mass flow rate at the condenser channels	\dot{m}_{Ci}	$kg\ s^{-1}$
Inlet mass flow rate at the evaporator channels	\dot{m}_{Ei}	$kg\ s^{-1}$
Outlet mass flow rate at the evaporator channels	\dot{m}_{Eo}	$kg\ s^{-1}$
Permeate output rate	\dot{m}_{pG}	$kg\ s^{-1}$
Pure water vapour pressure	$P_{v,w}$	Pa
Saltwater vapour pressure	$P_{v,sw}$	Pa
Specific thermal energy consumption	q_{STEC}	$kWh\ m^{-3}$
Convective heat flux from the condenser channel	q_C	Wm^{-2}
Condenser channel heat flux	\dot{q}_{cold}	Wm^{-2}
Convective heat flux from the evaporator channel	q_E	Wm^{-2}
Evaporator channel heat flux	\dot{q}_{hot}	Wm^{-2}
Heat transfer rate from the membrane surface	q_M	Wm^{-2}
Specific conductive heat flux	$\dot{q}_{M,C}$	Wm^{-2}
Specific latent heat flux	$\dot{q}_{M,L}$	Wm^{-2}
Salinity	S	$g\ kg^{-1}$
Feed water salinity in the input of the condenser channel	S_{Ci}	$g\ kg^{-1}$

Feed water salinity in the input of the evaporator channel	S_{Ei}	$g\ kg^{-1}$
Feed water salinity in the output of the evaporator channel	S_{Eo}	$g\ kg^{-1}$
Temperature at condenser inlet	T_{Ci}	$^{\circ}C$
Temperature at condenser outlet	T_{Co}	$^{\circ}C$
Temperature at evaporator inlet	T_{Ei}	$^{\circ}C$
Temperature at evaporator outlet	T_{Eo}	$^{\circ}C$
Temperature at the membrane surface on the evaporator side	T_{Me}	$^{\circ}C$
Temperature at the membrane surface on the permeate gap side	T_{Mp}	$^{\circ}C$
Temperature in permeate gap channel	T_{PG}	$^{\circ}C$
Permeate flow rate	V_p	$m^3\ s^{-1}$
Impermeable film thickness	δF	m
Membrane thickness	δ_m	m
Permeate gap thickness	δ_{PG}	m